Multi-plane and Multi-phase Unbalance Vibration Response and Coupling Characteristics of Inner and Outer Dual Rotor System

Gaoshan Wei [1, 2], Hao Zhang [1, 2], Pingping Ma [1], Jingyu Zhai [1, 2], Qingkai Han [1, 2*]

1 School of Mechanical Engineering, Dalian University of Technology, Dalian, China, 114026
2. Collaborative Innovation Center of Major Machine Manufacturing in Liaoning, Dalian, China, 114026

Abstract: In this paper, the dual rotor system of a turbofan aero engine, including an internal rotor and an external rotor, is simplified to a four-disc and five-supporting dual rotor system based on the dynamic similarity. The inherent characteristics, the unbalanced vibration responses and the coupling characteristics of the inner and outer dual rotor are analyzed. First, the low-pressure fan rotor, the high-pressure compressor, the high-pressure turbine and the low-pressure turbine of the aero engine are simplified into four mass equivalent and rotary inertia equivalent discs. Five supportings (front and rear supportings of fan rotor, rear supporting of low-pressure turbine rotor, front and rear supportings of high-pressure rotor), are replaced by springs with different stiffness, and a corresponding 5-supportings, 4-discs,3-axis dual rotor simplified dynamic model are set up. The motion differential equations of the inner and outer dual rotor system with 12 degrees of freedom is established using the *Lagrange equation*. Through analytical analysis for these equations, the inherent characteristics, the multi-plane and multi-phase unbalance vibration response of the different equivalent discs in various working conditions with different rotational speeds. The time-domain signal, frequency-domain signal, the rotating axis center locus and whirling locus are studied. The influence of the unbalanced mass magnitude and the unbalance mass phase difference between the fan disc and the high-pressure compressor disc on the coupling vibration of the dual rotor are analyzed. The results show that the disc centroid phases of the low-pressure rotor and the high-pressure rotor will reverse when the rotation speed goes through the critical speed of the dual rotor. The amplitude of the vibration response has a linear relationship with the magnitude of the imbalance. The unbalance phase difference between the high-pressure rotor and the low-pressure rotor has no effect on the coupling vibration of the dual rotor.

Keywords: Dual rotor; Multi-plane and multi-phase unbalance; Coupling characteristics; Analytical analysis

* Corresponding author (hanqingkai@dlut.edu.cn)

ISSN 2572-4975 (Print), 2572-4991 (Online)

1 Introduction

The inner and outer dual rotor system with intermediate bearing is generally adopted in medium-thrust or even bigger-thrust turbofan engines. This kind of structure can reduce the weight and improve the thrust-weight ratio. Compared to a support- independent rotor, high-pressure rotor and low-pressure rotor interact each other through the intermediate bearing which leads to the dynamic characteristics and the critical speed characteristics more complex.

The vibration of the aero engine rotor system will cause aircraft to stop in many cases, or even some more serious problems such as structural damage. The imbalance of the inner and outer dual rotor makes up a large majority of the engine vibration problems. However, the unique coupling characteristics of inner and outer dual rotor system cause the law of unbalanced vibration and its influencing factors more complex and not easy to grasp. Gupta et al. [1] studied the critical speed of the rotor, the modal shape and the mutual excitation between the rotors with the transfer matrix method. Chiang et al. [2] analyzed the natural frequency and critical speed of the single rotor and double rotor system with the finite element method, and calculated the stiffness of the bearing. In paper [3], a dual rotor-bearing-casing coupling dynamic model for aero engine was established using the finite element method. The nonlinear dynamic response of the system was obtained by numerical integration. Paper [4] studied the optimization of the dynamic characteristics of the four-supporting dual rotor system with a mediating supporting, and optimized the critical speed characteristics and damping characteristics of the system. Paper [5] studied the effect of supporting stiffness on the natural frequency and vibration mode of a double rotor with ANSYS software. In paper [6], the comparison between the complete method and the reduction method is made to calculate the critical speed of the dual rotor system. Paper [7] studied the steady-state unbalance response of an inverse rotation dual rotor engine by a theoretical and experimental methods. Paper [8] studied the beat vibration of the dual rotor system of an aero engine. In paper [9], the inherent characteristics of the dual rotors are analyzed and optimized, and the unbalance response is also analyzed by using the transfer matrix method. Paper [10] proposed a model based method of dual rotor unbalance fault diagnosis by using the transfer matrix method. Paper [11] analyzed the centroid trajectories of the dual rotor under the over-critical and non-over-critical stage.

At present, the transfer matrix method and the finite element method are mostly used in domestic study of dual rotor vibration. The study mainly includes the inherent characteristics and fault analysis of the dual rotor with some vibration response. However little research focus on the coupling characteristics of dual rotor unbalanced vibration.

In this paper, a simplified dynamics model of a rotor system composed of 5 supportings, 4 discs, and 3 shafts is established according to aero engine inner and outer dual rotor system. Different from transfer matrix method and finite element method, the basic theory of dynamics and the Lagrange equation was used to get the motion differential equations for this dual rotor system. Based on the differential equations, unbalanced vibration response and coupling characteristics of the dual rotor system were analyzed analytically. In this research, the effect of unbalance vibration on the vibration transmission of dual rotor can be found, as well as the influence of the mass magnitude

 ISSN 2572-4975 (Print), 2572-4991 (Online)

and imbalance phase difference between the internal rotor and external rotor on the vibration coupling of the dual rotor. In addition, it also provides a theoretical basis for the research of unbalance identification.

2 Dynamic model of the inner and outer dual rotor system

2.1 Simplification method

Figure 1 shows the rotor structure of a certain type of aero engine. The engine rotor system is made of a high-pressure rotor and a low-pressure rotor through an intermediate bearing, as well as including 6 supportings as shown in the figure. The high-pressure rotor consists of 2 supportings, 4# supporting and 5# supporting, and the supporting mode is 1-0-1 with 5# supporting an intermediate supporting. The low-pressure rotor consists of 4 supportings, 1# supporting, 2# supporting, 3# supporting and 6# supporting, and the supporting mode is 1-2-1. 2# supporting and 3# supporting are rigid support, so they were simplified to 1 rigid supporting in the simplified dynamics model.

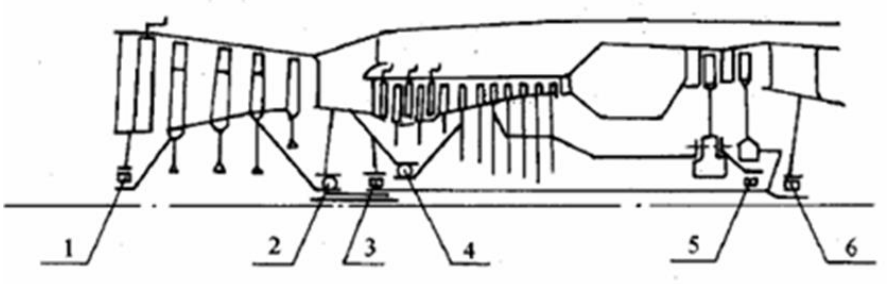

Fig. 1. The schematic diagram of the aero engine rotor system

The simplified model is shown in figure 2. Fan discs, low-pressure turbine disc, high-pressure compressor discs and high-pressure turbine disc in aero engine rotor are simplified to D_1, D_2, D_3, D_4 in the model respectively and form the 4-discs structure. The fan rotor and the low-pressure turbine rotor are connected by a coupling. High-pressure rotor and low-pressure turbine rotor are assembled together through the intermediate bearing. The equivalent stiffness K_{b2} in the dynamic model are calculated by the stiffness of 2# and 3# supporting in the prototype.

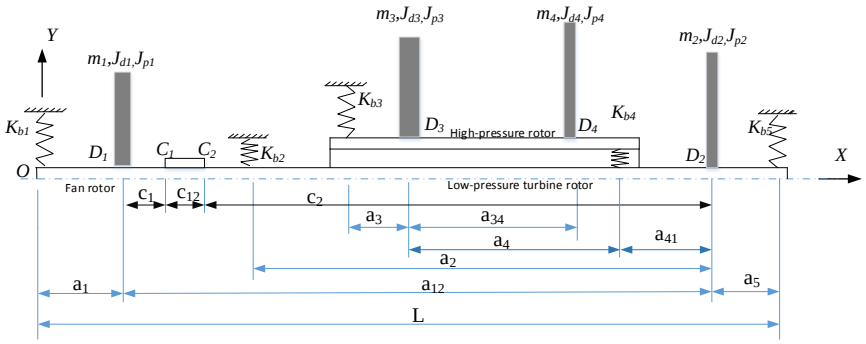

Fig. 2. The simplified dynamic model of rotor system

The simplified dynamic model is made of a high-pressure rotor and a low-pressure rotor.

The low-pressure rotor system consists of 2 rotating shafts, 2 discs, 3 supports and 1 coupling. These two shafts are connected by a coupling. The two discs are installed at D_1 of the fan rotor and D2 of the low-pressure turbine rotor respectively. The connection points of the coupling are C_1 and C_2 respectively. L is the total length of the low-pressure rotor; a_{12} is the center span of the two discs D_1 and D_2; a_1 the distance between D_1 and supporting B_1; a_2 is the distance between D_2 and supporting B_2; a_5 is the distance between D_2 and supporting B_5;

The high-pressure rotor consists of 1 rotating shaft, 2 discs and 2 supportings. 2 discs are installed at D_3 and D_4 respectively. a_3 is the distance between D_3 and supporting B_3; a_{34} is the distance between D_3 and D_4.

2.2 Basic differential equation of motion

According to the *Lagrange equation*, kinetic energy equations and potential energy equations of the mode should be first established, and then these equations are derived by each degree of freedom. At last, the dynamic equations of the dual rotor can be obtained.

2.2.1 The establishment of coordinate system

In figure 3, the fixed reference coordinate system *OXYZ* used in rotor system is marked, and it can be used to depict the position, speed and acceleration of the rotor system. The origin *O* of the coordinate system is a fixed point. Axis *OX* are parallel to the horizontal plane, coinciding with the rotating center line of the rotating shaft

For the dual rotor system, inertial spindle coordinate systems $D_1\xi\eta\zeta$ and $D\xi_2\eta_2\zeta_2$ of two discs and moving coordinate system $O_2X_2Y_2Z_2$ are established in addition to the fixed coordinate system. The detailed introduction are described as following.

ISSN 2572-4975 (Print), 2572-4991 (Online)

Rotating disc inertial spindle coordinate system $D_1\xi\eta\zeta$ is established in figure 3 and it can be transformed into the fixed coordinate system $OXYZ$ following some steps: the coordinate translate from $OXYZ$ to D_1XYZ, rotate around axis Z a angle θ_{z_1} and change into D_1x^*yZ, rotate around axis y a angle θ_{y_1} and change into D_1xyz, rotate around axis x a angle Ψ_1 and change into the inertial spindle coordinate system $D_1\xi\eta\zeta$ of the rotating disc 1.

According to these steps, the relationship between the unit vectors of the three rotating coordinate system $\boldsymbol{i}_m, \boldsymbol{j}_m, \boldsymbol{k}_m (m=1,2,3)$ and the unit vectors of the fixed coordinate system is shown as following.

$$\begin{bmatrix} \boldsymbol{i} \\ \boldsymbol{j} \\ \boldsymbol{k} \end{bmatrix} = \begin{bmatrix} \cos\theta_{z1} & -\sin\theta_{z1} & 0 \\ \sin\theta_{z1} & \cos\theta_{z1} & 0 \\ 0 & 0 & 1 \end{bmatrix} \begin{bmatrix} \boldsymbol{i}_1 \\ \boldsymbol{j}_1 \\ \boldsymbol{k}_1 \end{bmatrix} \approx \begin{bmatrix} \theta_{z1} & -\theta_{z1} & 0 \\ \theta_{z1} & \theta_{z1} & 0 \\ 0 & 0 & 1 \end{bmatrix} \begin{bmatrix} \boldsymbol{i}_1 \\ \boldsymbol{j}_1 \\ \boldsymbol{k}_1 \end{bmatrix} = \boldsymbol{T}_1 \begin{bmatrix} \boldsymbol{i}_3 \\ \boldsymbol{j}_3 \\ \boldsymbol{k}_3 \end{bmatrix} \tag{1}$$

$$\begin{bmatrix} \boldsymbol{i}_1 \\ \boldsymbol{j}_1 \\ \boldsymbol{k}_1 \end{bmatrix} = \begin{bmatrix} \cos\theta_{y1} & 0 & \sin\theta_{y1} \\ 0 & 1 & 0 \\ -\sin\theta_{y1} & 0 & \cos\theta_{y1} \end{bmatrix} \begin{bmatrix} \boldsymbol{i}_2 \\ \boldsymbol{j}_2 \\ \boldsymbol{k}_2 \end{bmatrix} \approx \begin{bmatrix} \theta_{y1} & 0 & \theta_{y1} \\ 0 & 1 & 0 \\ -\theta_{y1} & 0 & \theta_{y1} \end{bmatrix} \begin{bmatrix} \boldsymbol{i}_2 \\ \boldsymbol{j}_2 \\ \boldsymbol{k}_2 \end{bmatrix} = \boldsymbol{T}_2 \begin{bmatrix} \boldsymbol{i}_2 \\ \boldsymbol{j}_2 \\ \boldsymbol{k}_2 \end{bmatrix} \tag{2}$$

$$\begin{bmatrix} \boldsymbol{i}_2 \\ \boldsymbol{j}_2 \\ \boldsymbol{k}_2 \end{bmatrix} = \begin{bmatrix} 1 & 0 & 0 \\ 0 & \cos\Psi_1 & -\sin\Psi_1 \\ 0 & \sin\Psi_1 & \cos\Psi_1 \end{bmatrix} \begin{bmatrix} \boldsymbol{i}_3 \\ \boldsymbol{j}_3 \\ \boldsymbol{k}_3 \end{bmatrix} = \boldsymbol{T}_3 \begin{bmatrix} \boldsymbol{i}_3 \\ \boldsymbol{j}_3 \\ \boldsymbol{k}_3 \end{bmatrix} \tag{3}$$

where,

$$\boldsymbol{T}_1 = \begin{bmatrix} \theta_{z1} & -\theta_{z1} & 0 \\ \theta_{z1} & \theta_{z1} & 0 \\ 0 & 0 & 1 \end{bmatrix}, \quad \boldsymbol{T}_2 = \begin{bmatrix} \theta_{y1} & 0 & \theta_{y1} \\ 0 & 1 & 0 \\ -\theta_{y1} & 0 & \theta_{y1} \end{bmatrix},$$

$$\boldsymbol{T}_3 = \begin{bmatrix} 1 & 0 & 0 \\ 0 & \cos\Psi_1 & -\sin\Psi_1 \\ 0 & \sin\Psi_1 & \cos\Psi_1 \end{bmatrix}$$

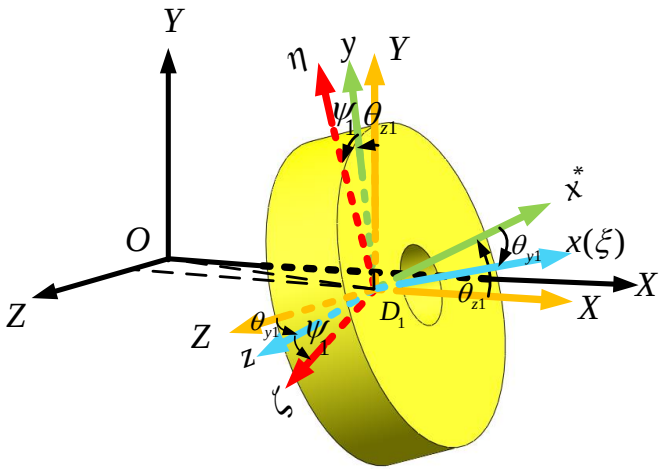

Fig. 3. Inertial spindle coordinate systems of the rigid disc

2.2.2 Kinetic energy and potential energy of the rotor system

According to the method for establishing coordinate system and the method for determining the generalized displacement and generalized velocity in chapter 2.2.1, kinetic energy and potential energy of the dual rotor system can be obtained.

(a) Total kinetic energy of the system

Total kinetic energy of the system is the sum of the translational kinetic energy and rotational kinetic energy of the four discs, and it can be written as

$$\begin{aligned}
\mathrm{T}&=T_{t1}+T_{r1}+T_{t2}+T_{r2}+T_{t3}+T_{r3}+T_{t4}+T_{r4}\\
&=\frac{1}{2}m_1\left(\dot{x}_1^{\,2}+\dot{y}_1^{\,2}+\dot{z}_1^{\,2}\right)+J_{p1}\Omega_1\theta_{z1}\dot{\theta}_{y1}+\frac{1}{2}J_{d1}\dot{\theta}_{y1}^{\,2}+\frac{1}{2}J_{d1}\dot{\theta}_{z1}^{\,2}+\frac{1}{2}J_{p1}\Omega_1^{\,2}\\
&+\frac{1}{2}m_2\left(\dot{x}_2^{\,2}+\dot{y}_2^{\,2}+\dot{z}_2^{\,2}\right)+J_{p2}\Omega_1\theta_{z2}\dot{\theta}_{y2}+\frac{1}{2}J_{d2}\dot{\theta}_{y2}^{\,2}+\frac{1}{2}J_{d2}\dot{\theta}_{z2}^{\,2}+\frac{1}{2}J_{p2}\Omega_1^{\,2}\\
&+\frac{1}{2}m_3\left(\dot{x}_3^{\,2}+\dot{y}_3^{\,2}+\dot{z}_3^{\,2}\right)+J_{p3}\Omega_3\theta_{z3}\dot{\theta}_{y3}+\frac{1}{2}J_{d3}\dot{\theta}_{y3}^{\,2}+\frac{1}{2}J_{d3}\dot{\theta}_{z3}^{\,2}+\frac{1}{2}J_{p3}\Omega_3^{\,2}\\
&+\frac{1}{2}m_4\left(\dot{x}_3^{\,2}+\left(\dot{\theta}_{z3}a_{34}+\dot{y}_3\right)^2+\left(-\dot{\theta}_{y3}a_{34}+\dot{z}_3\right)^2\right)+J_{p4}\Omega_3\theta_{z3}\dot{\theta}_{y3}+\frac{1}{2}J_{d4}\dot{\theta}_{y3}^{\,2}\\
&+\frac{1}{2}J_{d4}\dot{\theta}_{z3}^{\,2}+\frac{1}{2}J_{p4}\Omega_3^{\,2}
\end{aligned} \tag{4}$$

(b) The total elastic potential energy of the system

The total potential energy of the system consists of the elastic potential energy of 5 supportings and the potential energy of the coupling. The potential energy of the coupling is

$$\mathrm{U}_c=(q_{c1}-q_{c2})^T K(q_{c1}-q_{c2}) \tag{5}$$

ISSN 2572-4975 (Print), 2572-4991 (Online)

In this equation, q_{c1} and q_{c2} are the displacements of the C_1, C_2 at two ends of the coupling.

$$K=\begin{bmatrix} k_{cy} & 0 & 0 & 0 \\ 0 & k_{cz} & 0 & 0 \\ 0 & 0 & k_{c\theta y} & 0 \\ 0 & 0 & 0 & k_{c\theta z} \end{bmatrix} \tag{6}$$

The total potential energy of the system can be written as

$$\begin{aligned} U &= U_1+U_2+U_3+U_4+U_c+U_5 \\ &= \frac{1}{2}k_{b1x}x_1^{\,2}+\frac{1}{2}\left(-a_1\theta_{z1}+y_1\right)k_{b1y}\left(-a_1\theta_{z1}+y_1\right)+\frac{1}{2}\left(a_1\theta_{y1}+z_1\right)k_{b1z}\left(a_1\theta_{y1}+z_1\right)+\frac{1}{2}x_2^{\,2}k_{b2x} \\ &+\left(-\frac{1}{2}a_2\theta_{z2}+\frac{1}{2}y_2\right)k_{b2y}\left(-a_2\theta_{z2}+y_2\right)+\frac{1}{2}\left(a_2\theta_{y2}+z_2\right)k_{b2z}\left(a_2\theta_{y2}+z_2\right)+\frac{1}{2}x_3^{\,2}k_{b3x} \\ &+\frac{1}{2}\left(-\theta_{z3}a_3+y_3\right)k_{b3y}\left(-\theta_{z3}a_3+y_3\right)+\frac{1}{2}\left(\theta_{y3}a_3+z_3\right)k_{b3z}\left(\theta_{y3}a_3+z_3\right)+\frac{1}{2}x_2^{\,2}k_{b5x} \\ &+\frac{1}{2}\left(\theta_{z2}a_5+y_2\right)k_{b5y}\left(\theta_{z2}a_5+y_2\right)+\frac{1}{2}\left(-\theta_{y2}a_5+z_2\right)k_{b5z}\left(-\theta_{y2}a_5+z_2\right) \\ &+\frac{1}{2}\left(x_1-x_2\right)k_{cx}\left(x_1-x_2\right)+\frac{1}{2}\left(\theta_{z1}c_1+\theta_{z2}c_2+y_1-y_2\right)k_{cy}\left(\theta_{z1}c_1+\theta_{z2}c_2+y_1-y_2\right) \\ &+\frac{1}{2}\left(-\theta_{y1}c_1-\theta_{y2}c_2+z_1-z_2\right)k_{cz}\left(-\theta_{y1}c_1-\theta_{y2}c_2+z_1-z_2\right)+\frac{1}{2}\left(\theta_{y1}-\theta_{y2}\right)k_{c\theta y}\left(\theta_{y1}-\theta_{y2}\right) \\ &+\frac{1}{2}\left(\theta_{z1}-\theta_{z2}\right)k_{c\theta z}\left(\theta_{z1}-\theta_{z2}\right)+\frac{1}{2}\left(x_3-x_2\right)k_{b4x}\left(x_3-x_2\right) \\ &+\frac{1}{2}\left(\theta_{z2}a_{41}+\theta_{z3}a_4-y_2+y_3\right)k_{b4y}\left(\theta_{z2}a_{41}+\theta_{z3}a_4-y_2+y_3\right) \\ &+\frac{1}{2}\left(-\theta_{y2}a_{41}-\theta_{y3}a_4-z_2+z_3\right)k_{b4z}\left(-\theta_{y2}a_{41}-\theta_{y3}a_4-z_2+z_3\right)+\frac{1}{2}\left(\theta_{y3}-\theta_{y2}\right)k_{b4\theta y}\left(\theta_{y3}-\theta_{y2}\right) \\ &+\frac{1}{2}\left(\theta_{z3}-\theta_{z2}\right)k_{b4\theta z}\left(\theta_{z3}-\theta_{z2}\right) \end{aligned} \tag{7}$$

2.2.3 Establishment of the dual rotor dynamic equations

After simplifying and discreting the system, the system analytic model can be established by using the *Lagrange equation* as follows.

$$\frac{d}{dt}\frac{\partial T}{\partial \dot{q}_j}-\frac{\partial T}{\partial q_j}+\frac{\partial U}{\partial q_j}+\frac{\partial D}{\partial \dot{q}_j}=Q_j(t),\quad j=1,2,3\cdots \tag{8}$$

Here, q_j and $\dot{q}_j$ are generalized coordinates and generalized velocities respectively; *T* and *U* are the kinetic energy and potential energy of the system respectively; *D* is the energy dissipation function of the system; *Qj(t)* is the generalized external excitation force. If the work done by some exciting force has been expressed as the kinetic energy and potential energy form of the vibration system, or the form of energy dissipation function, then these exciting forces are no longer considered on the right side of the equation. In this rotor system, the influence of energy dissipation function D is neglected. Function (1) can be rewritten as

$$\frac{d}{dt}\frac{\partial T}{\partial \dot{q}_j}-\frac{\partial T}{\partial q_j}+\frac{\partial U}{\partial q_j}=Q_j(t),\quad j=1,2,3\cdots \tag{9}$$

Considering the motion equation of the rotor, and ignoring the external excitation. The differential equations of the system motion are derived and arranged as follows.

$$m_1\ddot{y}_1+k_{cy}\left(\theta_{z1}c_1+\theta_{z2}c_2+y_1-y_2\right)+k_{b1y}(y_1-a_1\theta_{z1})=0$$

$$m_1\ddot{z}_1+k_{cz}\left(-\theta_{y1}c_1-\theta_{y2}c_2+z_1-z_2\right)+k_{b1z}(z_1+a_1\theta_{y1})=0$$

$$J_{d1}\ddot{\theta}_{y1}+J_{p1}\Omega_1\dot{\theta}_{z1}+k_{cz}\theta_{y1}c_1^{\,2}-k_{cz}\left(-\theta_{y2}c_2+z_1-z_2\right)c_1$$
$$+\left(k_{b1z}a_1^{\,2}+k_{c\theta y}\right)\theta_{y1}+k_{b1z}a_1z_1-k_{c\theta y}\theta_{y2}=0$$

$$J_{d1}\ddot{\theta}_{z1}-J_{p1}\Omega_1\dot{\theta}y_1+k_{cy}c_1^{\,2}\theta_{z1}+k_{cy}\left(\theta_{z2}c_2+y_1-y_2\right)c_1$$
$$+\left(k_{b1y}a_1^{\,2}+k_{c\theta z}\right)\theta_{z1}-k_{b1y}a_1y_1-k_{c\theta z}\theta_{z2}=0$$

$$m_2\ddot{y}_2+\left(-k_{cy}c_2-k_{b2y}a_2-k_{b4y}a_{41}+k_{b5y}a_5\right)\theta_{z2}+k_{b4y}\left(-\theta_{z3}a_4+y_2-y_3\right)$$
$$+k_{cy}\left(-\theta_{z1}c_1-y_1+y_2\right)+\left(k_{b2y}+k_{b5y}\right)y_2=0$$

$$m_2\ddot{z}_2+\left(k_{cz}c_2+k_{b2z}a_2+k_{b4z}a_{41}-k_{b5z}a_5\right)\theta_{y2}+k_{b4z}\left(\theta_{y3}a_4+z_2-z_3\right)$$
$$+k_{cz}\left(\theta_{y1}c_1-z_1+z_2\right)+\left(k_{b2z}+k_{b5z}\right)z2=0$$

$$J_{d2}\ddot{\theta}_{y2}+J_{p2}\Omega_1\dot{\theta}_{z2}+\left(k_{cz}c_2^{\,2}+k_{b2z}a_2^{\,2}+k_{b4z}a_{41}^{\,2}+k_{b5z}a_5^{\,2}+k_{c\theta y}+q_{b4\theta y}\right)\theta_{y2}$$
$$+k_{b4z}\left(\theta_{y3}a_4+z_2-z_3\right)a_{41}-k_{cz}\left(-\theta_{y1}c_1+z_1-z_2\right)c_2+\left(k_{b2z}a_2-k_{b5z}a_5\right)z_2$$
$$-k_{c\theta y}\theta_{y1}-k_{b4\theta y}\theta_{y3}=0$$

$$J_{d2}\ddot{\theta}_{z2}-J_{p2}\Omega_1\ddot{\theta}_{y2}+\left(k_{cy}c_2^{\,2}+k_{b2y}a_2^{\,2}+k_{b4y}a_{41}^{\,2}+k_{b5y}a_5^{\,2}+k_{c\theta z}+k_{b4\theta z}\right)\theta_{z2}$$
$$+k_{b4y}\left(\theta_{z3}a_4-y_2+y_3\right)a_{41}+k_{cy}\left(\theta_{z1}c_1+y_1-y_2\right)c_2+\left(-k_{b2y}a_2+k_{b5y}a_5\right)y_2$$
$$-k_{c\theta z}\theta_{z1}-k_{b4\theta z}\theta_{z3}=0$$

$$\left(m3+m4\right)\ddot{y}_3+m_4a_{34}\ddot{\theta}_{z3}+k_{b4y}\left(\theta_{z2}a_{41}+\theta_{z3}a_4-y_2+y_3\right)-k_{b3y}\theta_{z3}a_3+k_{b3y}y_3=0$$

$$\left(m_3+m_4\right)\ddot{z}_3-m_4a_{34}\ddot{\theta}_{y3}+k_{b4z}\left(-\theta_{y2}a_{41}-\theta_{y3}a_4-z_2+z_3\right)+k_{b3z}\theta_{y3}a_3+k_{b3z}z_3=0$$

ISSN 2572-4975 (Print), 2572-4991 (Online)

$$\begin{aligned}
&\left(m_4 a_{34}{}^2 + J_{d3} + J_{d4}\right)\ddot{\theta}_{y3} - m_4 a_{34}\ddot{z}_3 + \left(J_{p3} + J_{p4}\right)\Omega_3\dot{\theta}_{z3} + a_4{}^2 k_{b4z}\theta_{y3} \\
&+k_{b4z}\left(\theta_{y2}a_{41} + z_2 - z_3\right)a_4 + \left(k_{b3z}a_3{}^2 + k_{b4\theta y}\right)\theta_{y3} + k_{b3z}a_3 z_3 - k_{b4\theta y}\theta_{y2} = 0 \\
&\left(m_4 a_{34}{}^2 + J_{d3} + J_{d4}\right)\ddot{\theta}_{z3} + m_4 a_{34}\ddot{y}_3 - \Omega_3\left(J_{p3} + J_{p4}\right)\dot{\theta}_{y3} + k_{b4y}a_4{}^2\theta_{z3} \\
&+k_{b4y}\left(\theta_{z2}a_{41} - y_2 + y_3\right)a_4 + \left(k_{b3y}a_3{}^2 + k_{b4\theta z}\right)\theta_{z3} - k_{b3y}a_3 y_3 - k_{b4\theta z}\theta_{z2} = 0
\end{aligned} \tag{10}$$

3 Dynamic characteristics and critical speeds of the inner and outer dual rotor system

3.1 Calculating method

This chapter mainly calculates the dynamic characteristics and critical speeds of the dual rotor, according to equations (10) and the basic parameters, dynamic characteristics and critical rotational speeds of low-pressure rotor, high-pressure rotor, inner and outer dual rotor are analyzed. The parameters needed in the calculating are shown as follows.

Table 1. Disk mass parameters

Disc name	Mass (Kg)	Moment of inertia of diameter (Kg m^2)	Polar moment of inertia (Kg m^2)
Fan disc	m_1=99.8	J_{d1}=4.18	J_{p1}=5.029
Low pressure turbine disc	m_2=69.2	J_{d2}=1.859	J_{p2}=3.69
High pressure compressor disc	m_3=143.1	J_{d3}=5.428	J_{p3}=5.567
High pressure turbine disc	m_4=101.1	J_{d4}=2.738	J_{p4}=5.431

Table 2. Stiffness of the supportings

1# supporting	2# supporting	3# supporting	4# supporting	5# supporting
3.3e7 N/m	2.5e8 N/m	3.3e7 N/m	2.5e8 N/m	3.3e7 N/m

Table 3. The length parameters

Parameters	Value(m)	Parameters	value(m)

a1	0.326	a41	0.029
a2	0.887	a5	0.160
a3	0.137	c1	0.305
a34	0.513	c2	1.323
a4	0.874	c12	0.136

Taking the basic parameters into the equations, eigenvalues and eigenvectors can be calculated, and the natural frequencies of the rotor and the corresponding modes of vibration can be obtained. Solving the frequency at a given speed, and Campbell diagram and critical speed can be obtained.

3.2 The critical speed calculation of low-pressure rotor and high-pressure rotor

According to the dynamic differential equations of the simplified dynamic model, the critical speed of low-pressure rotor and high-pressure rotor can be calculated through *MATLAB* programming.

3.2.1 Inherent characteristics of low-pressure rotor

Removing the effect of the high pressure rotor in the dynamic differential equations, and the critical speed of low pressure rotor can be calculated. The calculating results of Campbell diagram and critical speed are shown in Fig. 4 and Table.4.

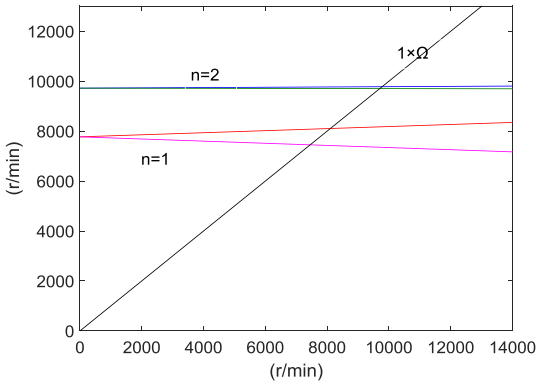

Fig. 4. Campbell diagram of low-pressure rotor

According to Campbell diagram, the intersections of the straight line with slope 1 and the positive precession line, the negative precession line are the critical speeds of the rotor. The critical speed of the rotor is shown in table .4.

Table 4. Critical speeds of high-pressure rotor

ISSN 2572-4975 (Print), 2572-4991 (Online)

1th order critical speeds/rpm	2nd order critical speeds/rpm
8123	9756
7200	9500

3.2.2 Inherent characteristics of high-pressure rotor

Removing the effect of the low-pressure rotor in the dynamic differential equations, and the critical speed of high-pressure rotor can be calculated.

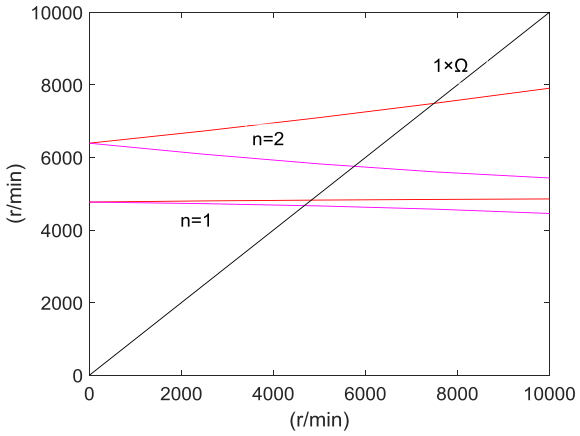

Fig. 5. Campbell diagram of high-pressure rotor

According to Campbell diagram, the intersections of the straight line with slope 1 and the positive precession line, the negative precession line are the critical speed of the rotor. The critical speed of the rotor is shown in table 5.

Table 5. Critical speeds of high-pressure rotor

1th order critical speeds/rpm	2nd order critical speeds/rpm
4800	7500
4750	5920

3.3 Inherent characteristics of inner and outer dual rotor

In this section, the inherent characteristics of the inner and outer dual rotor are calculated, and the calculated results are shown in Fig.6. Fig. 6(a) shows the 1th order vibration mode of dual rotor, and Fig. 6(b) shows the 2th order vibration mode. It can be seen that the 1th vibration mode of high-pressure rotor is a translational mode, and the 1th order vibration mode of low-pressure rotor is the pitching vibration mode; the 2th order modes of high-pressure rotor and low-pressure rotor are all pitching vibration mode.

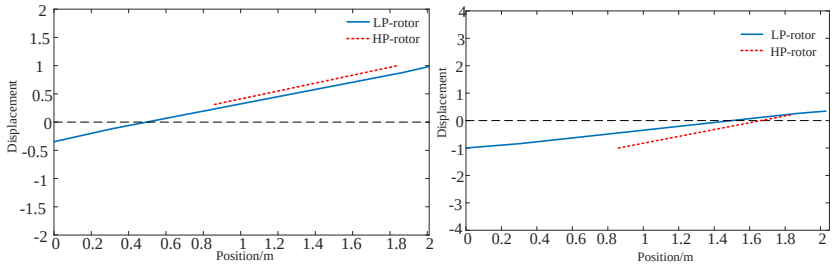

（a）1th order vibration mode（79.6Hz）（b）2nd order vibration mode（95Hz）

Fig. 6. Vibration mode of dual rotor

Through calculating the whirl frequencies of dual rotor at different rotational speeds, Campbell diagram can be drawn and the critical speed can be calculated. Fig.7 is the Campbell diagram of dual rotor when the rotation speed ratio of low-pressure rotor and high-pressure rotor is 1.

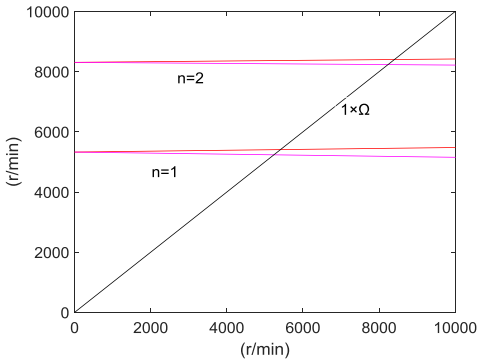

Fig. 7. Campbell diagram of inner and outer dual rotor

According to Campbell diagram, the intersections of the straight line with slope 1 and the positive precession line, the negative precession line are the critical speed of the rotor. The critical speed of the rotor is shown in table.6.

Table 6. Critical speeds of dual rotor

1th order critical speeds/rpm	2nd order critical speeds/rpm
5270	8204
5020	7920

4 Multi-plane and multi-phase unbalance vibration response

Because of the interaction of high-pressure rotor and low-pressure rotor, the unbalance vibration response of inner and outer dual rotor is very complex. In this section,

ISSN 2572-4975 (Print), 2572-4991 (Online)

unbalanced vibration response of high-pressure rotor and low-pressure rotor are analyzed under sub-critical and over-critical conditions considering the interaction of the two rotors. The sub-critical and over-critical conditions respectively refer to the stage of a slightly lower speed than the critical speed and a slightly higher speed than the critical speed. The sub-critical speeds and over-critical speeds are shown in the table 7. The working speed of the aero engine is between 2nd and 3rd critical speed, so in this section only the first two critical speeds are analyzed. The basic imbalance of the disc is 40 gmm.

Table 7. The rotation speed under sub-critical and over-critical conditions

The critical order	Rotation speed
1st critical speed	5270 rpm
1st sub-critical speed	5000 rpm
1st over-critical speed	5500 rpm
2nd critical speed	8204 rpm
2nd sub-critical speed	8000 rpm
2nd over-critical speed	8500 rpm

4.1 Unbalanced vibration response of low-pressure rotor under sub-critical and over-critical conditions

The low-pressure rotor consists of 3 supportings, 2 discs and 1 coupling. In this section, unbalanced vibration responses of low-pressure rotor at sub-critical and over-critical conditions are analyzed with the high-pressure rotor speed 0 rpm. The unbalanced mass exerted on the low-pressure fan disk is 40 gmm. The unbalance response analysis results of the low-pressure rotor is shown as following.

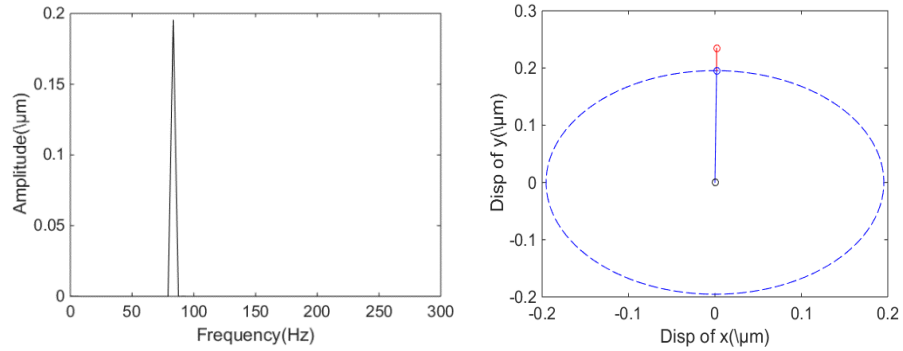

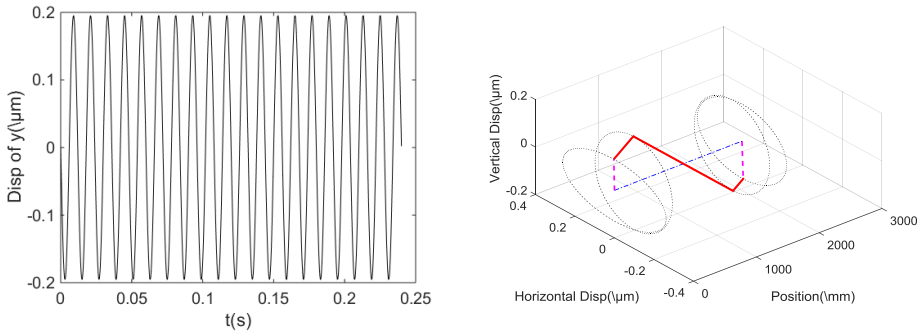

Fig. 8. 1th order sub-critical unbalance response of low-pressure rotor

It can be seen from Fig.8, the unbalanced vibration response frequency of the low-pressure rotor at 1th sub-critical state is mainly the rotational frequency of the rotor. The phases of the centroid and mass center of the disc are almost the same. The time-history response is periodic. The whirl vibration mode of the rotating shaft is mainly the pitching mode.

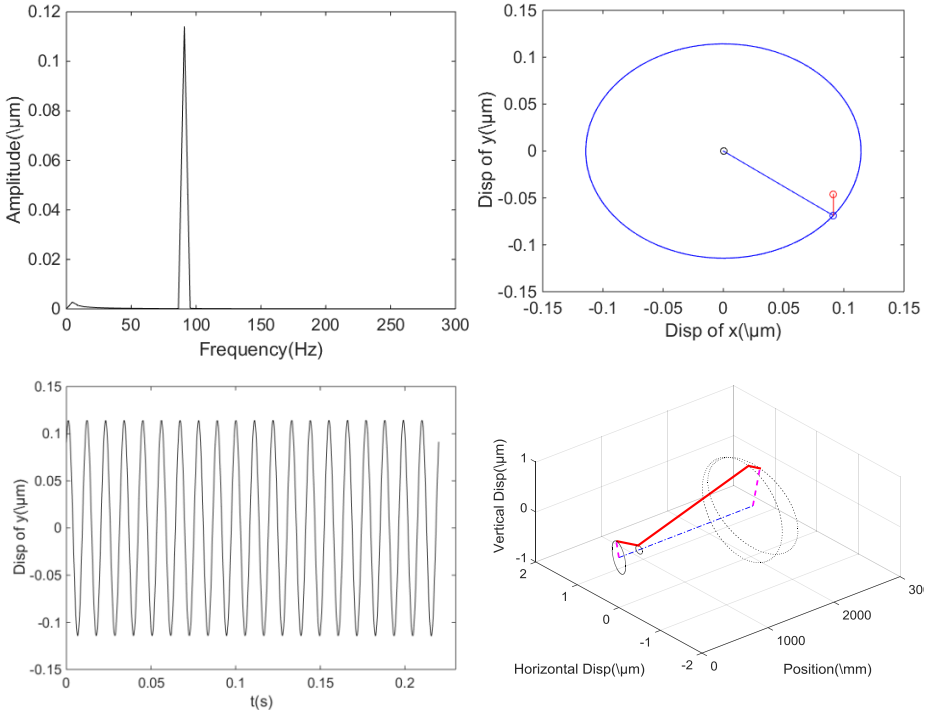

Fig. 9. 1th order over-critical unbalance response of low-pressure rotor

It can be seen from Fig.9, the unbalanced vibration response frequency of the low-pressure rotor at 1th over-critical state is mainly the rotational frequency of the rotor.

ISSN 2572-4975 (Print), 2572-4991 (Online)

The phase difference of the centroid and mass center of the disc is among 90° and 180° . The time history response is periodic. The whirl vibration mode of the rotating shaft is mainly the translational mode.

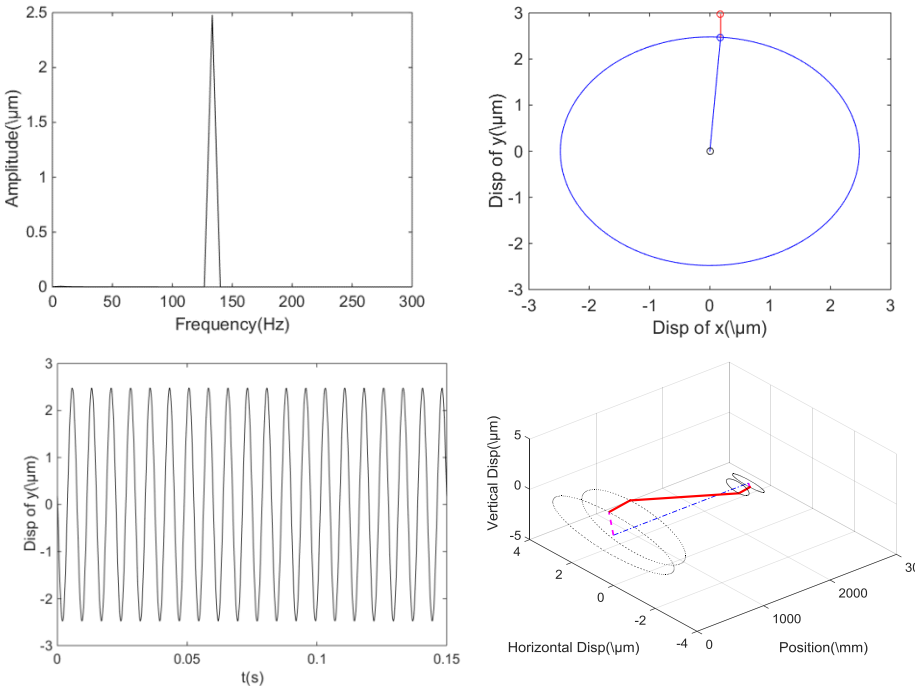

Fig. 10. 2nd order sub-critical unbalance response of low-pressure rotor

It can be seen from Fig.10, the difference between the phase of centroid and the phase of mass center at the 2nd sub-critical stage reverses, and the whirl vibration mode is the pitching mode.

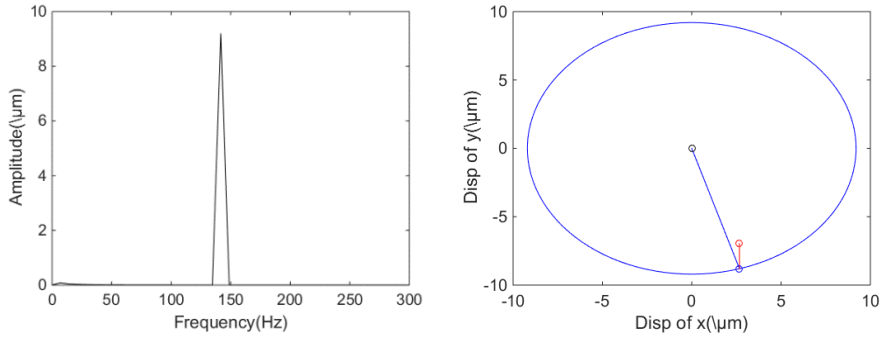

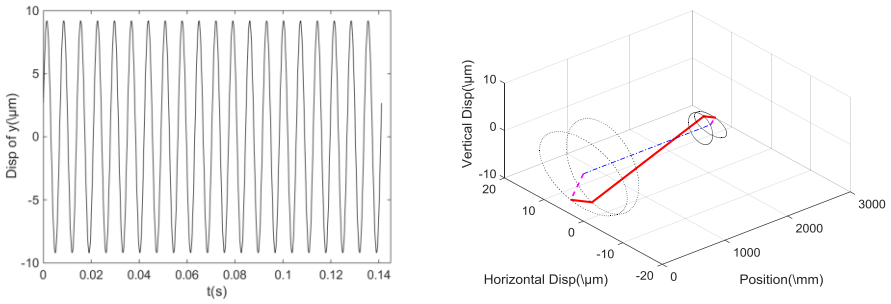

Fig. 11. 2nd order over-critical unbalance response of low-pressure rotor

The phase difference between the centroid and mass center of the disc reverses again at the 2nd over-critical stage. The whirl vibration mode of the rotating shaft is the pitching mode.

4.2 Unbalanced vibration response of high-pressure rotor under sub-critical and over-critical conditions

The high-pressure rotor consists of 2 supportings and 2 discs. In this section, unbalanced vibration response of high-pressure rotor at 1st sub-critical stage, 1st over-critical stage, 2nd sub-critical stage and 2nd over-critical stage is analyzed when the rotating speed of low-pressure rotor is 0. Based on the equations (10), the unbalanced mass exerted on the high-pressure fan disk is 40 gmm, and the unbalance-vibration-response analysis results of high-pressure compressor disc is shown in Fig.12.

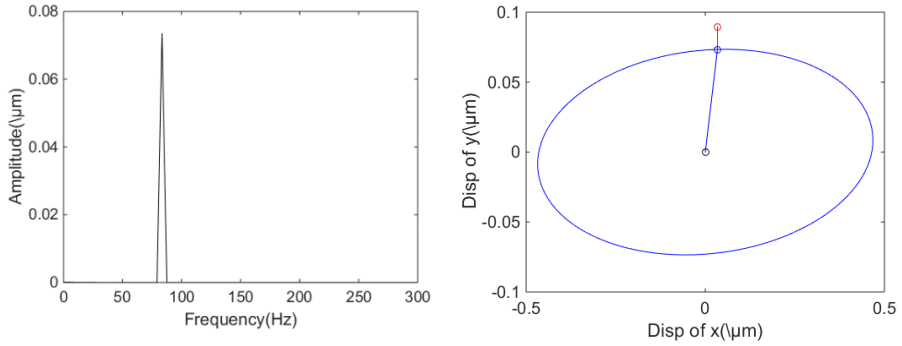

ISSN 2572-4975 (Print), 2572-4991 (Online)

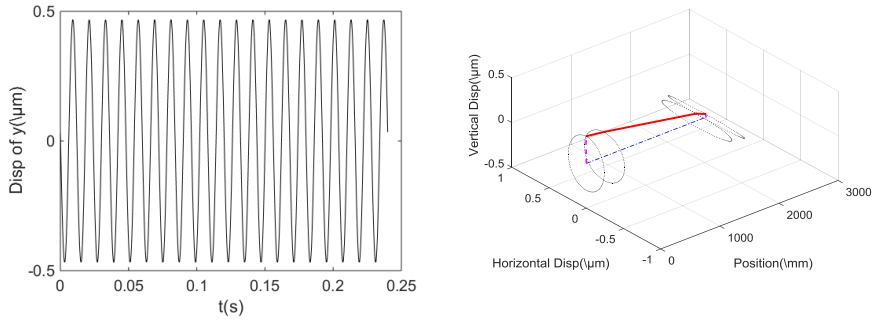

Fig. 12. 1th order sub-critical unbalance response of high-pressure rotor

It can be seen from Fig.12, the unbalanced vibration response frequency of the high-pressure rotor at 1th subcritical state is mainly the rotational frequency of the rotor. The phase of the centroid and mass center of the disc is almost the same. The time history response is periodic. The whirl vibration mode of the rotating shaft is mainly the translational mode.

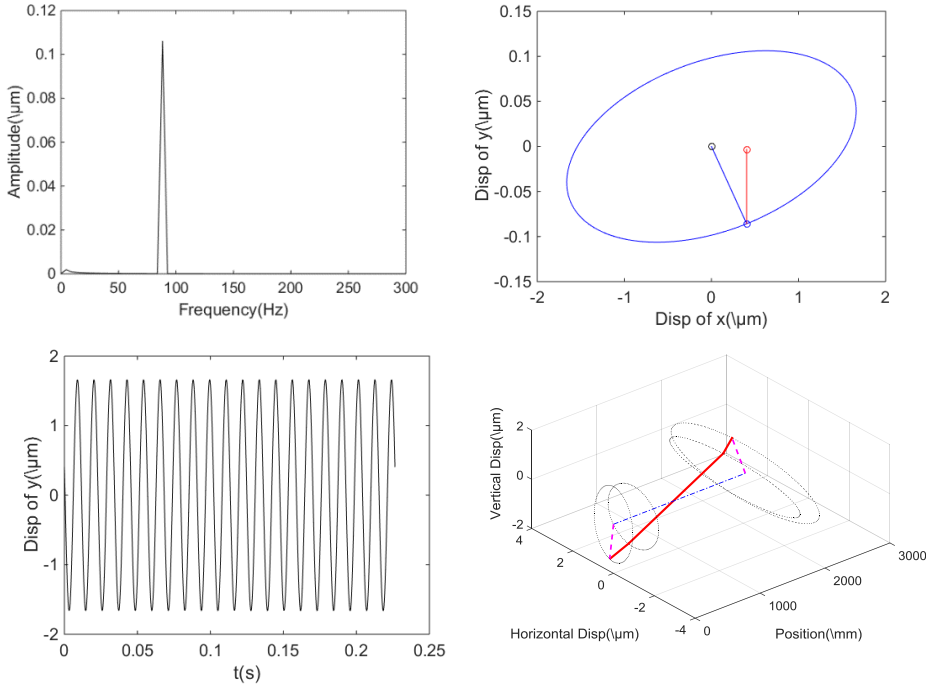

Fig. 13. 1th order over-critical unbalance response of high-pressure rotor

It can be seen from Fig.13, the unbalanced vibration response frequency of the high-pressure rotor at 1th over-critical state is mainly the rotational frequency of the rotor. The phase difference of the centroid and mass center of the disc is almost 180 °which

means that the phase reverse happens. The time history response is periodic. The whirl vibration mode of the rotating shaft is mainly the pitching mode.

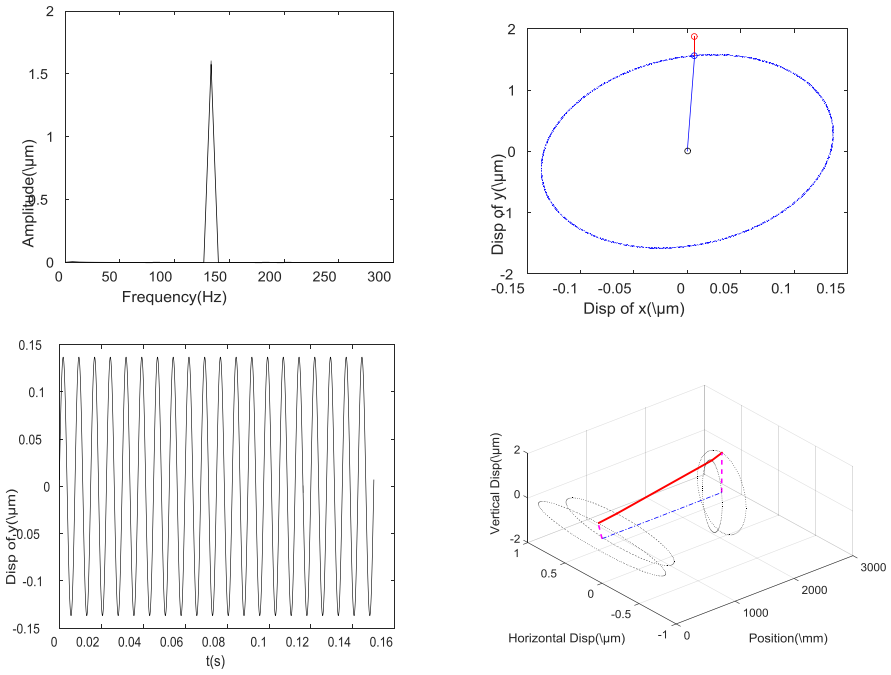

Fig. 14. 2nd order sub-critical unbalance response of high-pressure rotor

It can be seen from Fig.14, the unbalanced vibration response frequency of the high-pressure rotor at 2nd sub-critical state is mainly the rotational frequency of the rotor. The phase of the centroid and mass center of the disc is almost the same. The phase reverse happens compared to 1th over-critical state. The whirl vibration mode of the rotating shaft is mainly the translation mode.

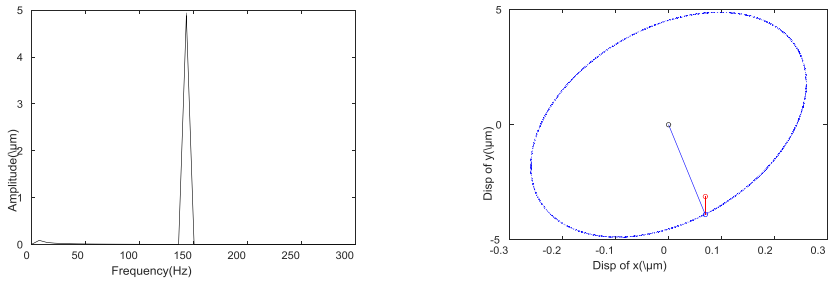

ISSN 2572-4975 (Print), 2572-4991 (Online)

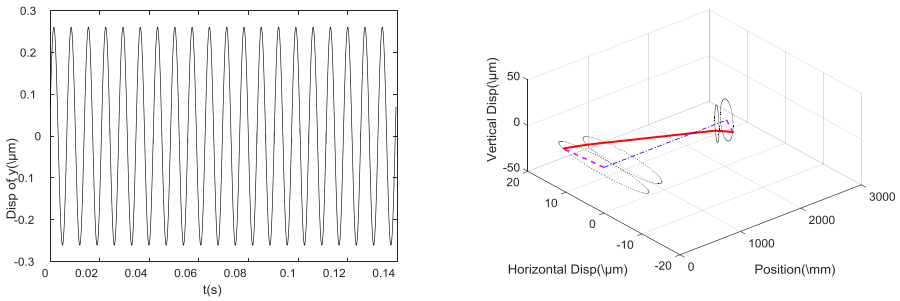

Fig. 15. 2nd order over-critical unbalance response of high-pressure rotor

It can be seen from Fig.15, The phase reverses again compared to 2nd sub-critical state. The whirl vibration mode of the rotating shaft changes into pitching mode.

To sum up, comparing the unbalanced vibration response at four different speeds, the phase difference of the mass center and the centroid have reversed when the rotation speed goes through the 1st and the 2nd critical speed. The whirl vibration mode at the 1th and 2nd sub-critical states are both the translational modes, and changing into the pitching modes at the 1th and 2nd over-critical stage.

5 Analysis of inner and outer dual rotor unbalanced vibration coupling and vibration transmission

In this chapter, based on the equations (10), inner and outer dual rotor unbalanced vibration coupling and vibration transfer are analyzed with New-mark method. The vibration amplitudes at the testpoints in the model are calculated, and then the influence of unbalanced mass and phase difference of high-pressure rotor and low-pressure rotor on vibration coupling and vibration transmission are studied.

5.1 Effect of unbalanced mass on vibration and vibration transmission of dual rotor

Aero engine low-pressure fan and high-pressure compressor section are both composed of multi-stage blisk-drums, and low-pressure turbine and high-pressure turbine are both composed of 1 turbine blisk. The unbalanced mass of high-pressure turbine disc and low-pressure turbine disc are very smaller than those of the low-pressure fan disc and the high-pressure compressor disc, so in this chapter only the unbalanced mass of the low-pressure fan disc and the high-pressure compressor disc are considered. The two aspects of influence, the unbalanced mass and the phase difference of the unbalanced mass, are studied to analyze the vibration response of the dual rotor

5.1.1 The influence of the fan disc unbalanced mass on the vibration and vibration transmission of dual rotor

In this section, the influence of the disc unbalanced mass on the vibration and vibration transmission of dual rotor are analyzed under 4 different rotation speeds. The rotation speeds are listed in table 8. Imposing imbalances 40*i（i=1, 2, 3 ……）gmm on the fan disk. The imbalance imposed on high-pressure compressor disc is 0. Through calculating the vibration amplitudes at the testpoints in the model, the unbalanced vibration transferring law is analyzed. The testpoints and its distribution are shown in Table. 9 and Fig.16.

Table 8. Working rotation speed

Number of the rotation speed	Low-pressure rotor/LP	High-pressure rotor/HP
1	3000 r/min	5000 r/min
2	5000 r/min-	7000 r/min
3	7000 r/min	9000 r/min
4	9000 r/min	11000 r/min

Table 9. Testpoints list

Testpoint number	Testpoint location
1	1#supporting
2	Fan disc
3	Low-pressure turbine disc
4	5#supporting
5	3#supporting
6	High-pressure compressor disc
7	High-pressure turbine disc
8	4#supporting

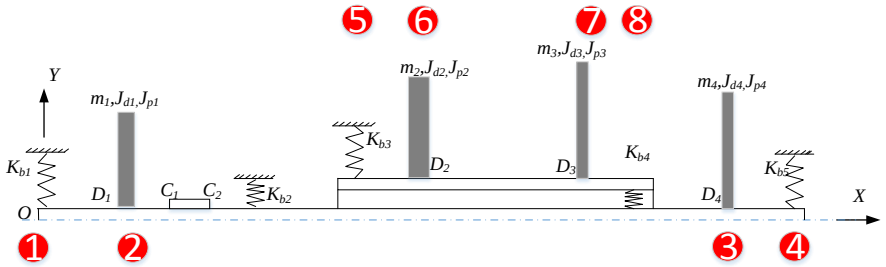

FFig. 16. The unbalanced response of testpoint distribution

According to the calculated vibration amplitude of each testpoint, the vibration amplitudes of the testpoints can be drawn into curves at different rotating speeds with different imbalances. The results are shown as below.

ISSN 2572-4975 (Print), 2572-4991 (Online)

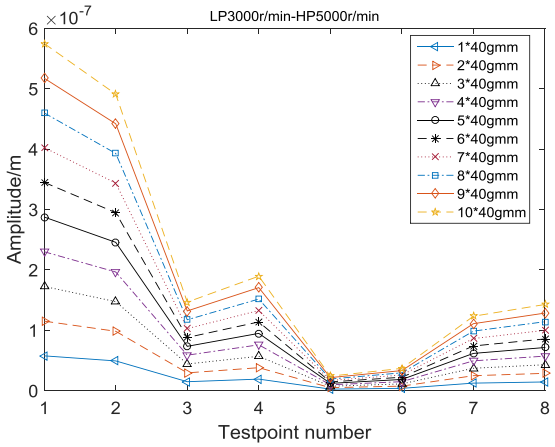

Fig. 17. The vibration amplitudes of the testpoints at 1# rotation speed

It can be seen from Fig. 17, the amplitude magnitude of the unbalanced vibration response has a linear relationship with the unbalanced mass. The amplitude of the response increases with the increase of unbalanced mass. Unbalanced mass is applied to the fan disc, that is, the 2# position of the testpoints. Under the condition of low-pressure rotor 3000 r/min and high-pressure rotor 5000 r/min, the vibration is reduced when transferred to the high-pressure rotor. The maximum vibration appears at fan disc and the minimum vibration appears at the front supporting of high-pressure rotor.

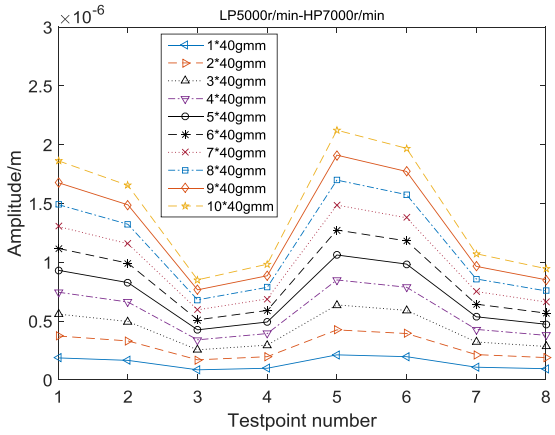

Fig. 18. The vibration amplitudes of the testpoints at 2# rotation speed

Under the condition of low-pressure rotor rotation speed 5000r/min and high-pressure rotor rotation speed 7000r/min. The unbalance vibration will stimulate the vibration in high-pressure rotor which may be caused by the rotation frequency close to the critical speed of high-pressure rotor. The maximum vibration appears at the front supporting of the high-pressure rotor, and the minimum vibration amplitude appears at low-pressure turbine disc.

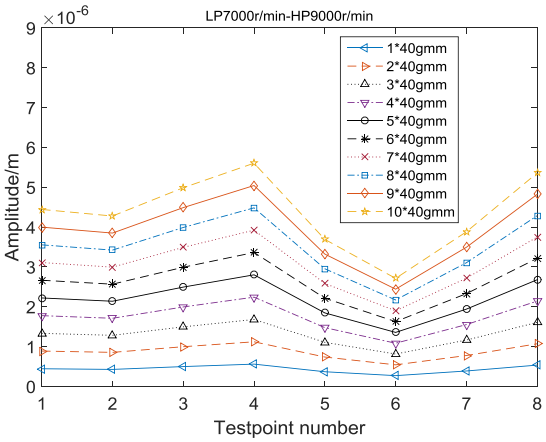

Fig. 19. The vibration amplitudes of the testpoints at 3# rotation speed

Under the condition of low-pressure rotor rotation speed 7000 r/min and high-pressure rotor rotation speed 9000 r/min, the unbalance vibration will also stimulate the vibration in high-pressure rotor. The maximum vibration appears at the rear supporting of the low-pressure rotor, and the minimum vibration amplitude appears at high-pressure turbine disc.

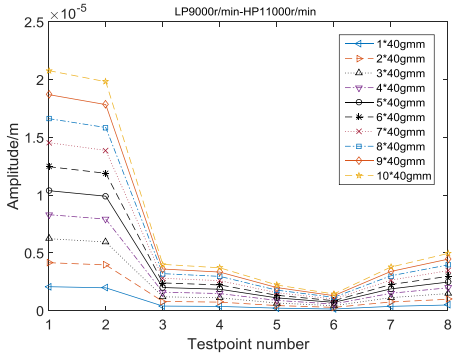

Fig. 20. The vibration amplitudes of the testpoints at 4# rotation speed

Under the condition of low-pressure rotor rotation speed 9000 r/min and high-pressure rotor rotation speed 11000 r/min, the vibration is reduced when transferred to the high-pressure rotor. The maximum vibration appears at the rear supporting of the low-pressure rotor, and the minimum vibration amplitude appears at high-pressure turbine disc.

Comparing the vibration responses under 4 different rotation speeds, it can be seen that the amplitude magnitude of the unbalanced vibration response has a linear relationship with the unbalanced mass. The unbalance vibration will stimulate the vibration in high-pressure rotor which may be caused by the rotation frequency close to the critical speed of high-pressure rotor.

ISSN 2572-4975 (Print), 2572-4991 (Online)

5.1.2 Influence of high-pressure compressor unbalanced mass on vibration and vibration transfer of dual rotor

Imposing imbalances 40*i（i =1, 2, 3 ……）gmm on the high-pressure turbine disc. The imbalance imposed on low-pressure rotor disc is 0. Through calculating the vibration amplitudes at the testpoints in the model, the unbalanced vibration transferring law is analyzed.

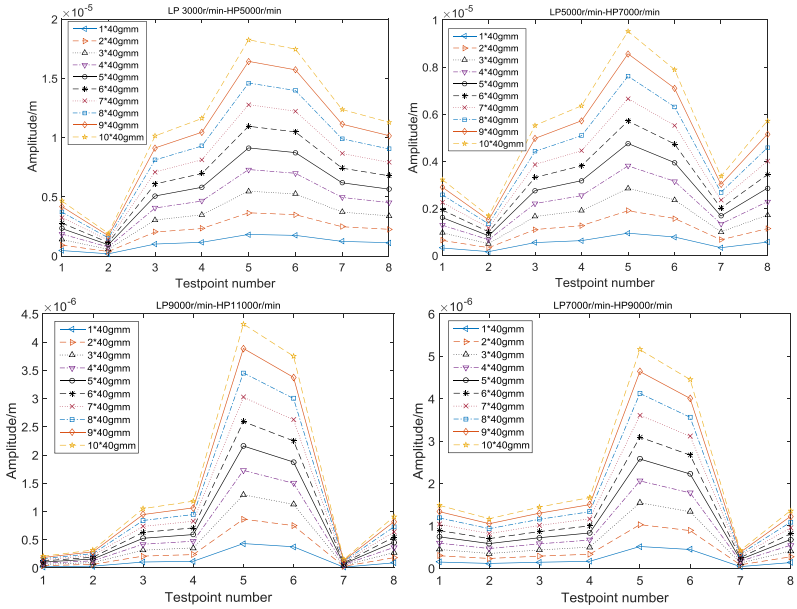

Fig. 21. Vibration amplitude of each testpoint at 4 different rotation speeds

As can be seen from Fig.21, the amplitude magnitude of the unbalanced vibration response has a linear relationship with the unbalanced mass. The unbalanced mass is imposed on the fan disc (6# testpoint). Under these 4 rotation speeds, the maximum vibration amplitude appears at the front supporting of the high-pressure rotor, and the vibration will reduce when it transfers to the low-pressure rotor. In this section, the unbalance response at a certain rotation speed can be analyzed, and providing a reference for the design of the aircraft engine.

5.2 Influence of unbalanced mass phase difference on vibration and vibration transmission of dual rotor

The influence of the phase difference between fan disc unbalanced mass and high-pressure compressor disc unbalanced mass on the vibration amplitude and vibration transmission of dual rotor is analyzed. Both fan disc and high-pressure compressor disc have an imbalance 40gmm. The unbalance vibration response is analyzed under 4 different rotation speeds when the phase difference is changed from 0° to 360°with a degree-step 10° .

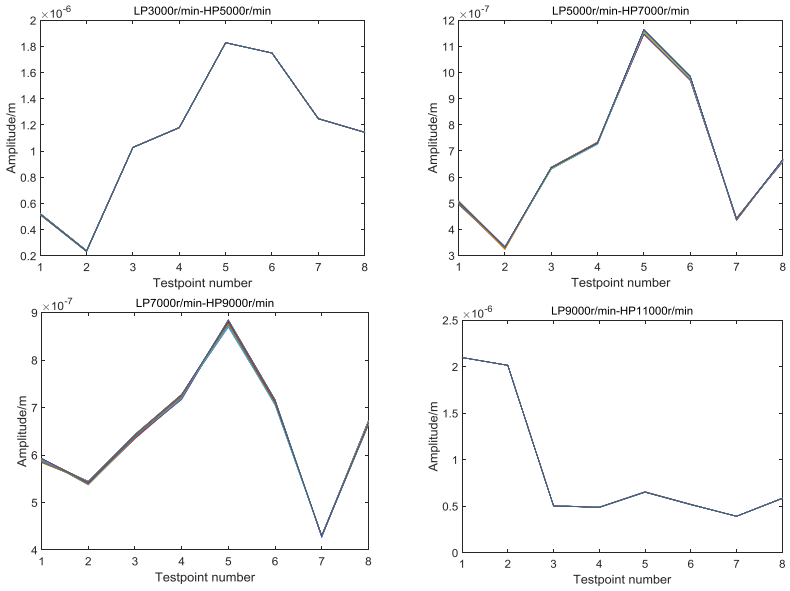

Fig. 22. Vibration amplitude of each testpoint under the condition of different phase differences at 4 different rotation speeds

There are 36 lines in each of the figure. However, as can be seen in the figures, these lines are overlap which means that unbalanced mass phase difference between low-pressure rotor and high-pressure rotor basically does not affect the vibration response when the rotation of the two rotors are different. In addition, the response amplitudes are different with the rotation speed changing.

6 Conclusions

This paper is based on the principle of mass and moment of inertia equivalent. The dual rotor dynamic model for aero engine is established and the motion differential equations of the dual rotor system are obtained through the basic theory of rotor dynamics and the *Lagrange equation*. The New-mark numerical integration method is used to solve the equations, and the inherent characteristics, vibration coupling and vibration transfer of the dual rotor are analyzed in an analytical point of view. The analysis results are shown below.

The unbalanced vibration amplitude of the dual rotor has a linear relationship with the magnitude of the unbalance mass.

Considering the interaction of the dual rotor, the phases difference between mass center and centroid of the disc in low-pressure rotor and high-pressure rotor will both reverse when the rotation speed goes through the critical speed.

ISSN 2572-4975 (Print), 2572-4991 (Online)

The unbalanced vibrations of the high-pressure rotor and the low-pressure rotor affect each other, the unbalance vibration of the high-pressure rotor will cause the vibration of the low pressure rotor, and low-pressure rotor has a similar effect on high-pressure.

References

1. K.G.D.G. Athre, Unbalance Response of a Dual Rotor System: Theory and Experiment, ***Journal of Vibration & Acoustics,*** 115 (1993) 427-435.
2. H.W.D. Chiang, C.N. Hsu, W. Jeng, et al., Turbo machinery Dual Rotor-Bearing System Analysis, ***ASME Turbo Expo 2002: Power for Land, Sea, and Air,*** (2002) 803-810.
3. G. Chen, Vibration modeling and analysis of dual rotor aero-engine system, ***Journal of Vibration Engineering***, 24 (2011) 619-632.
4. F. Wang, ***Dynamic performance optimization of four-supporting dual rotor with intermediate supporting***, Nanjing University of Aeronautics & Astronautics, 2012.
5. M. Shen, J.S. Tang, K.A. Li, et al., Modal analysis of the aero engine dual rotor system. ***Ordnance Industry Automation***, 29 (2010) 34-36.
6. D.Y. Zhang, Y.H. Liu, Z.C. Liang, et al., A method for calculating critical speed of aero engine dual rotor system, ***Journal of Propulsion Technology***, 36 (2015) 292-298.
7. G.Q. Feng, L.X. Zhang, F. Yi, Unbalance response of a reverse rotating dual rotor engine in steady state, ***Chinese Society for Vibration Engineering***, 1999.
8. J. Han, D.P. Gao, X.Hu, et al., Beat vibration analysis of dual rotor system for aero engine, ***Chinese Journal of Aeronautics***, 28 (2007) 1369-1373.
9. W.C. Zhan, Design optimization and unbalanced response analysis of dual rotor system, ***Huazhong University of Science and Technology***, 2014.
10. J. Han, D.P. Gao, X.Hu, A model-based dual rotor unbalance fault diagnosis method, ***Journal of Aerospace Power***, 23 (2008) 932-938.
11. C. Meng, G.H. Luo, Experimental research on the inner and outer rotor reverse imbalance response of two dual rotor systems with different structures, ***National Symposium on rotor dynamics***, 2012.